Electronic Supplementary Material (ESI) for Journal of Materials Chemistry C.

Supplementary Information

High-loading ultrastable $CsPbBr_3$ perovskite quantum dots in hierarchical Silicalite-1 by elimination of co-templates for multimodal optical applications

Xiandi Yu, Yuchi Zhang, Le Han, Yan Xu*

Department of Chemistry, College of Sciences, Northeastern University, Shenyang, Liaoning 110819, China

Figure Captions

Fig. S1. SEM images of (**a**) $CsPbBr_3$/Silicalite-1 (A-1), (**b**) $CsPbBr_3$/Silicalite-1 (A-2), and (**c**) $CsPbBr_3$/Silicalite-1 (A-3).

Fig. S2. (**a**) SEM, (**b**) TEM, (**c,d**) HRTEM images of $CsPbBr_3$/Silicalite-1 (A-4) nanocomposite.

Fig. S3. SEM images of (**a**) $CsPbBr_3$/Silicalite-1 (C-2-3), and (**b**) $CsPbBr_3$/Silicalite-1 (B-2-3).

Fig. S4. PL intensity stability of (**a**) $CsPbBr_3$/Silicalite-1 (B), and (**b**) $CsPbBr_3$/Silicalite-1 (C) nanocomposite when exposed in air and water, respectively.

Fig. S5. PL intensity stability of $CsPbBr_3$/Silicalite-1 (A-2-3) in solvent of DMSO, DMF, MeOH, EtOH, Acetone, and Hexane, respectively.

Fig. S6. Fingerprint stability of $CsPbBr_3$/Silicalite-1 (A-2-3) composite when exposed in air (**a-c**) and water (**d-f**), respectively.

Table S1 Comparison of BET surface areas and pore volumes of Silicalite-1, Silicalite-1 (A), and $CsPbBr_3$/Silicalite-1 (A-2-3).

Table S2 Comparison of temperature sensitivity of several $CsPbBr_3$-based optical thermometers for temperature sensing application.

Table S3 Comparison of Fe^{3+} detection for various materials based on different methods.

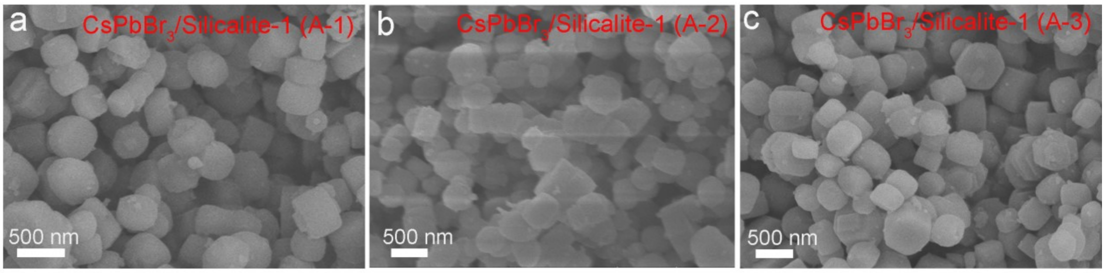

Fig. S1. SEM images of (**a**) $CsPbBr_3$/Silicalite-1 (A-1), (**b**) $CsPbBr_3$/Silicalite-1 (A-2), and (**c**) $CsPbBr_3$/Silicalite-1 (A-3).

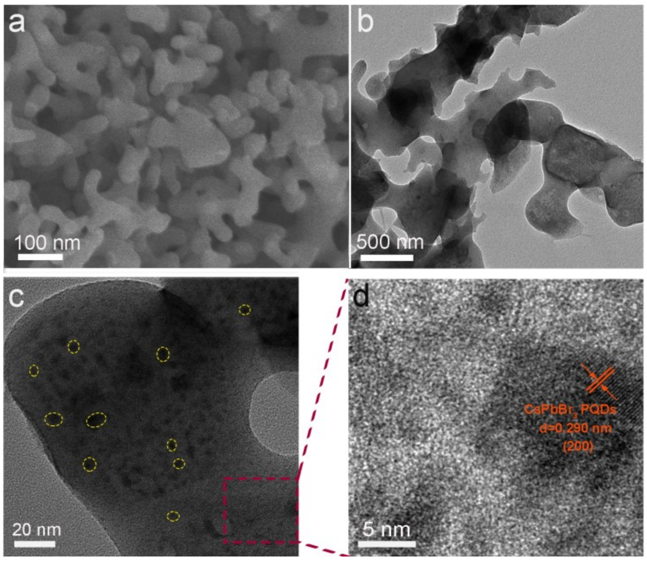

Fig. S2. (**a**) SEM, (**b**) TEM, (**c,d**) HRTEM images of $CsPbBr_3$/Silicalite-1 (A-4) nanocomposite.

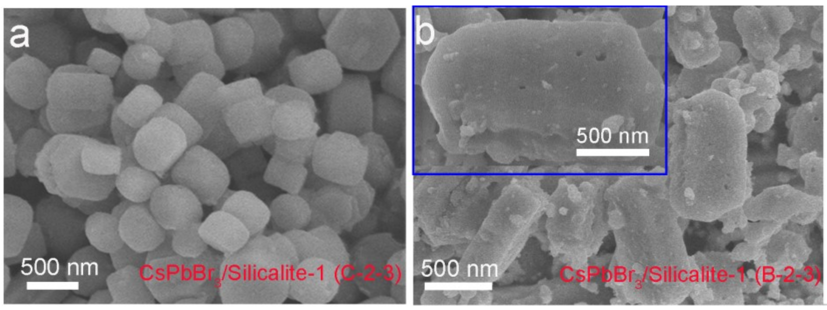

Fig. S3. SEM images of (**a**) $CsPbBr_3$/Silicalite-1 (C-2-3), and (**b**) $CsPbBr_3$/Silicalite-1 (B-2-3).

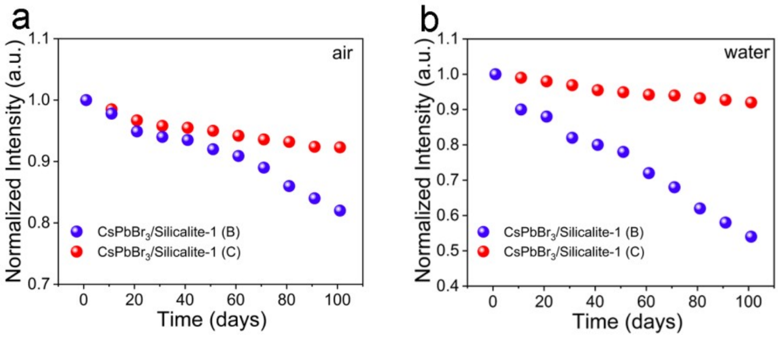

Fig. S4. PL intensity stability of (**a**) $CsPbBr_3$/Silicalite-1 (B), and (**b**) $CsPbBr_3$/Silicalite-1 (C) nanocomposite when exposed in air and water, respectively.

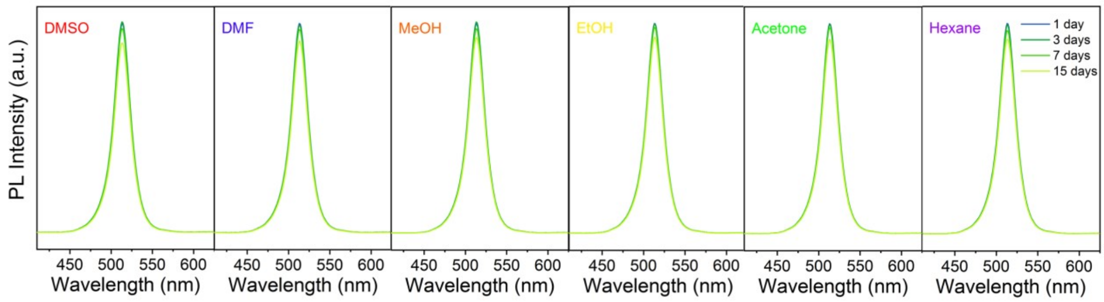

Fig. S5. PL intensity stability of $CsPbBr_3$/Silicalite-1 (A-2-3) in solvent of DMSO, DMF, MeOH, EtOH, Acetone, and Hexane, respectively.

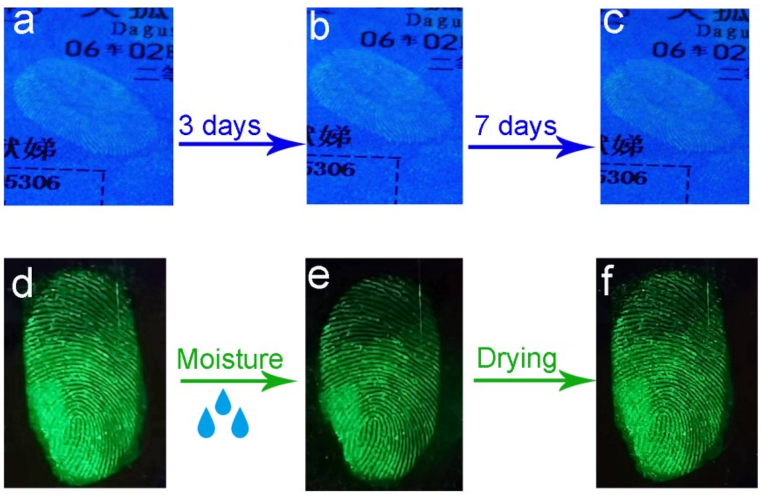

Fig. S6. Fingerprint stability of $CsPbBr_3$/Silicalite-1 (A-2-3) composite when exposed in air (**a-c**) and water (**d-f**), respectively.

Table S1 Comparison of BET surface areas and pore volumes of Silicalite-1, Silicalite-1 (A), and $CsPbBr_3$/Silicalite-1 (A-2-3).

Samples	S_{BET} (m^2/g)	S_{ext} (m^2/g)	V_{total} (cm^3/g)	V_{meso} (cm^3/g)	V_{micro} (cm^3/g)
Silicalite-1	428	63	0.267	0.093	0.174
Silicalite-1 (A)	249	275	0.68	0.69	-0.02
$CsPbBr_3$/Silicalite-1 (A-2-3)	565	378	0.958	0.877	0.08

Table S2 Comparison of temperature sensitivity of several $CsPbBr_3$-based optical thermometers for temperature sensing application.

Materials	Temp. range [°C]	Max. S_r [% $°C^{-1}$] or nm $°C^{-1}$	Ref.
$CsPbBr_3$/Silicalite-1 (A-2-3)	30-110	23 (110 °C)	This work
Tb^{3+}:$CsPbI_3$	(-193)-207	1.78 (107 °C)	[1]
$CsPbBr_3$-KSF-PS	30-70	10.31 (45 °C)	[2]
$CsPbBr_3$/$EuPO_4$	30-210	1.8 (150 °C)	[3]
$CsPbBr_3$/Eu^{3+}	30-120	2.11 (120 °C)	[4]
Dual-phase compounds of $NaYF_4$: Ho^{3+} and $CsPbBr_3$	20-160	5.13 (120 °C)	[5]
Eu^{3+}-doped $CsPbBr_3$ PQDs@glass	(-180)-110	2.25 (39 °C)	[6]
$CsPbBr_3$-TS-1	(-193)-107	7.14 (107 °C)	[7]
$CsPbBr_3$/Silicalite-1 (A-2-3)	30-110	0.079 nm $°C^{-1}$	This work
$CsPbBr_3$-TS-1	(-193)-107	0.035 nm $°C^{-1}$	[7]
$CsPbBr_3$-HSZ ZSM-5	10-100	0.073 nm $°C^{-1}$	[8]
$Dye_{0.001}$@Eu-MOF	10-90	0.142 nm $°C^{-1}$	[9]

Table S3 Comparison of Fe^{3+} detection for various materials based on different methods.

Material	Detection methods	Detection range (μM)	Detection limits (μM)	Ref.
Organic/inorganic hybrid titanium Oxide	Potentiometric detection	$1\text{-}10^4$	-	[10]
C dots	Ratiometric fluorescent sensing	5-50	0.16	[11]
ADTC functionalized Ag NPs	Colorimetric detection	2.49-69.8	6.18	[12]
Hyperbranched polyimide	Fluorescent sensing	0-600	60.6	[13]
Graphene quantum dots (GQDs)	Fluorescent sensing	3.5-670	1.6	[14]
SiO_2@$CsPbX_3$@SiO_2	Fluorescent sensing	10-70	3	[15]
$CsSnCl_3$ NCs by Bone Gelatin	Fluorescent sensing	0-2000	8	[16]
$CsPbBr_3$/Silicalite-1 (A-2-3)	Fluorescent sensing	$0.1\text{-}10^5$	0.78×10^{-3}	This work

References

[1] Y. Zhang, J. Liu, H. Zhang, Q. Ye, X. Liang, W. Xiang, Ultra-stable Tb^{3+}: $CsPbI_3$ nanocrystal glasses for wide-range high-sensitivity optical temperature sensing. J. Eur. Ceram. Soc. 40 (2020) 6023-6030.

[2] J. Jin, J. Lin, Y. Huang, L. Zhang, Y. Jiang, D. Tian, F. Lin, Y. Wang, X. Chen, High sensitivity ratiometric fluorescence temperature sensing using the microencapsulation of $CsPbBr_3$ and K_2SiF_6:Mn^{4+} phosphor. Chin. Chem. Lett. 33 (2022) 4798-4802.

[3] C. Wang, H. Lin, X. Xiang, Y. Cheng, Q. Huang, Y. Gao, X. Cui, Y. Wang, $CsPbBr_3$/$EuPO_4$ dual-phase devitrified glass for highly sensitive self-calibrating optical thermometry. J. Mater. Chem. C 6 (2018) 9964-9971.

[4] C. Lu, Y. Duan, P. Li, Y. Lu, S. Xu, J. Zhang, Polychromatic tunable luminescence of Eu^{3+} doped $CsPbBr_3$ quantum dot glass ceramic induced by mechanical crystallization. Ceram. Int. 48 (2022) 13826-13832.

[5] P. Lu, L. Lin, Z. Li, Z. Feng, Y. Yang, J. Cai, Z. Wang, Z. Zheng, Highly sensitive temperature sensing of compound of $CsPbBr_3$ perovskite quantum dots and $NaYF_4$:Ho^{3+} nanoparticles. Optik 246 (2021) 167794.

[6] X. Li, Y. Yu, J. Hong, Z. Feng, X. Guan, D. Chen, Z. Zheng, Optical temperature sensing of Eu^{3+}-doped oxyhalide glasses containing $CsPbBr_3$ perovskite quantum dots. J. Lumin. 219 (2020) 116897.

[7] L. Han, Y. Han, J. Wu, X. Zhang, Z. Wang, Y. Xu, Two-step in situ synthesis of $CsPbX_3$@TS-1 zeolite (X = Cl, Br, I) nanocomposites for optical thermometric, latent fingerprints and anti-counterfeiting applications. Mater. Chem. Front. 5 (2021) 7843-7851.

[8] Y. Zhang, L. Han, B. Li, Y. Xu, Improved stability of all-inorganic perovskite nanocrystals in hierarchical ZSM-5 zeolites for multimodal applications. Chem. Eng. J 437 (2022) 135290-135303.

[9] J. Liu, X. Yue, Z. Wang, X. Zhang, Y. Xu, Coumarin 7 functionalized europium-based metal-organic-framework luminescent composites for dual-mode optical thermometry. J. Mater. Chem. C 8 (2020) 13328-13335.

[10] M. Becuwe, P. Rouge, C. Gervais, M. Courty, A. Dassonville-Klimpt, P. Sonnet, E. Baudrin, A new sensitive organic/inorganic hybrid material based on titanium oxide for the

potentiometric detection of Iron (III). J. Colloid Interf. Sci. 388 (2012) 130-136.

[11] Q. An, Q. Lin, X. Huang, R. Zhou, X. Guo, W. Xu, S. Wang, D. Xu, H-T Chang, Electrochemical synthesis of carbon dots with a stokes shift of 309 nm for sensing of Fe^{3+} and ascorbic acid. Dyes Pigments 185 (2021) 108878-108886.

[12] S. Bothra, J.N. Solanki, S.K. Sahoo, J.F. Callan, Anion-driven selective colorimetric detection of Hg^{2+} and Fe^{3+} using functionalized silver nanoparticles. RSC Adv. 4 (2014) 1341-1346.

[13] A. Xing, X. Miao, T. Liu, H. Yang, Y. Meng, X. Li, An intrinsic white-light-emitting hyperbranched polyimide: synthesis, structure-property and its application as a "turn-off" sensor for iron (III) ions. J. Mater. Chem. C 7 (2019) 14320-14333.

[14] Y. Zhang, X. Yang, Y. Pu, W. Cheng, S. Lin, Z. Shao, X. Laio, Selective, sensitive and label-free detection of Fe^{3+} Ion in tap water using highly fluorescent graphene quantum dots. J Fluoresc. 29 (2019) 541-548.

[15] X-H. Tan, G-B. Huang, Z-X. Cai, F-M. Li, Y-M. Zhou, M-S. Zhang, Monodisperse spherical sandwiched structured SiO_2@$CsPbX_3$@SiO_2 perovskite composites for the determination of Fe^{3+} ion in water samples. J. Anal. Test 5 (2021) 40-50.

[16] D. G, Y. Zhang, B. Lyu, X. Guo, Y. Hou, J. Ma, B. Yu, S. Chen, Encapsulation of Pb-free $CsSnCl_3$ perovskite nanocrystals with bone gelatin: Enhanced stability and application in Fe^{3+} sensing. Inorg. Chem. 61 (2022) 6547-6554.